High precision mass measurements of 29-33Mg and the shell-opening effect at N=20

David Lunney, Georges Audi, Michel De Saintsimon, Carole Gaulard, Catherine Thibault, Nelson Vieira

EPJ manuscript No.
(will be inserted by the editor)

High precision mass measurements of $^{29-33}$Mg and the shell-opening effect at N = 20

D. Lunney, G. Audi, M. de Saint Simon, C. Gaulard, C. Thibault, N. Vieira and the ISOLDE Collaboration

Centre de Spectrométrie Nucléaire et de Spectrométrie de Masse (CSNSM)
IN2P3/CNRS-Université Paris Sud, Bâtiment 108, F-91405 Orsay, France

October 11, 2004

Abstract.
High precision mass measurements have been performed on the exotic magnesium isotopes $^{29-33}$Mg using the MISTRAL radiofrequency spectrometer, especially suited to very short-lived nuclides. This method, combined with the powerful tool of resonant laser ionization at ISOLDE, has provided a significant reduction of uncertainty for the masses of the most exotic Mg isotopes: a relative error of 7×10^{-7} was achieved for the weakly produced ^{33}Mg that has a half-life of only 90 ms. Moreover, the mass of ^{33}Mg is found to change by over 250 keV. Verifying and minimizing binding energy uncertainties in this region of the nuclear chart is important for understanding the phenomenon of shell opening: the lack of binding energy that is normally associated with magic numbers.

PACS. 21.10.Dr Binding energies and masses – 27.30.+t $20 \leq A \leq 38$ nuclides – 29.30.Aj charged particle spectrometers: electric and magnetic

1 Introduction

Shell structure is a pillar on which much of our knowledge and understanding of the nucleus rests. For some time now there has been evidence that this pillar is being eroded as the nuclear configuration tends towards the extreme in isospin. This is, of course, an allusion to the infamous "island of inversion," discovered long ago from an anomaly in the binding energies of exotic Na isotopes from $N = 19 - 21$ [1] . Binding energy that should normally be gained by the $N = 20$ shell closure is, in fact, unavailable, resulting rather in a shell "opening". Since that time, further investigation of binding energies far from stability have shown that the $N = 8$ [2,3] and the $N = 28$ [4] shell closures also succomb. However, where one magic number might disappear, it now seems that another can appear elsewhere - a veritable magic number *migration*. Such is the case for $N = 16$ [2], $Z = 16$, $N = 30$ [5], as well as $N = 32$ [6–8] and $N = 34$ [9,10] around $Z = 23$. Another magic appearance, claimed from gamma-ray spectroscopy at $Z = 28$, $N = 40$ [11], is particularly interesting since there is no corroborating evidence from binding energy data.

The island of inversion itself has since been the subject of intense experimental and theoretical scrutiny. A concise, historical review of the numerous expeditions devoted to its exploration is given in [12]. [1] The general consensus is that the island is a result of the inversion of so-called "intruder" configurations that formed by promoting a pair of neutrons across the $N = 20$ shell gap into the normally-empty fp shell. The intruder configurations are strongly deformed, resulting in a particularly interesting example of shape coexistence. More recent theoretical works have tackled the $N = 20$ shell-opening problem from the perspective of a strongly attractive component of the spin-isospin part of the effective nucleon-nucleon interaction [15–17], as well as a mean-field model with separable monopole interaction [18]. Promising efforts include important pairing correlations, either within the mean-field (HFB+QRPA) approach [19] or from Nuclear Field Theory [20] (in the case of $N = 8$).

Intense radioactive beams, coupled with powerful experimental techniques, have been brought to bear – not only on this recalcitrant island, but also magic number re-incarnations in general – in attempts to understand the cause. Since the original work of Detraz et al. [21] and

Send offprint requests to: lunney@csnsm.in2p3.fr

[1] Note that a reference was overlooked in that work (as in many papers) to an analysis based on binding energy differences by Heyde and Wood [13] who argued for shape coexistence in this region, a conclusion reached independently by the more often-cited shell-model calculations of Warburton, Becker and Brown [14].

Guillemaud-Mueller et al. [22], $\beta-$spectroscopy studies of ^{33}Mg have followed at ISOLDE [23] and MSU [24]. Interaction cross-section measurements have been performed at RIKEN for N =16 [2]. The new tool of neutron knockout [25] gives detailed information concerning initial- and final-state wave functions. New results from inelastic scattering [26] have also become available in the meantime (see [27] for a summary of direct reactions performed in the $N = 20$ region). Precision measurements of the quadrupole moments of $^{26-31}$Na (at ISOLDE) using a $\beta-$NMR, optical pumping technique by Keim et al. [28], provides a very important complementary perspective. The same technique has been used very recently to measure the magnetic moment of ^{31}Mg and unambiguously determine the spin [29].

A fine example of the application of a new technique can be found in the suite of papers by Pritychenko et al., [30–34] who performed $\gamma-$spectroscopy at MSU via intermediate energy, heavy-ion scattering off high-Z targets where Coulomb excitation is thought to be the dominant mechanism. The heavy ions in question are exotic nuclides produced upstream by fragmentation. These studies have provided a mapping of the shore of the island of inversion, corroborating that indicated by binding energies, as well as furnishing detailed nuclear structure information, especially concerning deformation. Coulomb excitation at fragmentation energies has been performed on ^{30,32}Mg at GANIL [35]. At RIKEN, γ-ray spectroscopy of ^{34}Mg, also produced by fragmentation, have yielded the energy of a 2^+ level [36] and the $B(E2)$ value of this state, determined by Coulomb excitation, yields an even larger deformation than for ^{32}Mg [37]. Particularly interesting is the recent result on ^{30}Mg from REX-ISOLDE [38]: a $B(E2)$ value that is a factor of two less than that of MSU [30] and a factor of three less than that of GANIL [35] (an almost 5σ deviation). While this result is preliminary, it indicates that the situation is considerably more complicated than previously assumed.

These new probes indeed shed more light on the shell opening phenomenon even if the data are somewhat lacking in precision. However, the methods would still seem not yet free of systematic error, the understanding of which is crucial for making any progress. Precision – and accuracy – are qualities of capital importance for measurements in general. It is therefore interesting to return to the original probe of the binding energy and make more precise measurements in order to put tighter constraints on the burgeoning theoretical approaches needed to interpret the data.

1.1 Mass measurements and the migration of magic numbers

Mass measurements play an underpinning role in this game of magic number hide and seek. It is often said that the atomic mass, through the binding energy $B(N, Z)$, embodies the net result of all interactions at work in the atom. This includes, of course, shell structure which is plainly visible when inspecting a graph of the two-neutron separation energy, defined by

$$S_{2n}(N, Z) = B(N, Z) - B(N - 2, Z) \qquad (1)$$

versus the number of neutrons, N for elements near the valley of stability. (The one-neutron separation energy is a less clear-cut indicator because of the pairing effect - another such embodiment.)

For a given Z, the general tendency for S_{2n} is to fall steadily as N increases. At the magic numbers (N_0) there is a sudden drop, corresponding to a loss in energy necessary to remove neutrons after a closed shell, before the more gradual fall resumes. The situation is well illustrated in Fig. 1, where we show the variation with neutron number of S_{2n} for the light elements up to $Z \sim 50$ (note that N is plotted on a logarithmic scale for easier comparison). The magic number $N_0 = 50$ is quite evident. At $N_0 = 28$ we see a similar manifestation, though less prounounced than the $N_0 = 50$ case. At $N_0 = 20$, however, the situation is far from obvious. This is partly due to another embodiment of nuclear structure in the binding energy for $N = Z$ nuclides (marked by a diamond in Fig.1), the so-called Wigner effect where the same type of kink that manifests a shell closure can be seen. For $N = Z = 20$, the Wigner effect coincides with the $N = 20$ shell closure but for lighter elements, their manifestation is difficult to discern. Note that since S_{2n} is a derivative of the mass surface, two discontinuities will result from a change due to nuclear structure: one where the phenomenon occurs and another two neutrons later (by definition). For $Z = 15 - 20$, the corresponding second kink is visible at $N = 22$ however it is only for $Z = 15, 16$ that the shell closure kink itself at $N_0 = 20$ is perceivable and for lower Z, it seems to have melted away. Whence, the discovery of the famous island [1].

The magic numbers were established from the earliest days of the shell model around 1950, at which time the data were limited to nuclei lying close to the valley of beta stability. It is natural to wonder, therefore, to what extent these numbers remain magic as one climbs towards the drip lines. Alternately, we can try to quantify the extent to which these erstwhile magic numbers have been "quenched," i.e., weakened or extinguished. A derivative of the S_{2n}, the shell gap, defined by:

$$\Delta_n(N, Z) = S_{2n}(N, Z) - S_{2n}(N + 2, Z) \qquad (2)$$

is a preferable way to examine questions of shell quenching. The shell gap (as calculated from experimental masses) is plotted in Fig. 2 as a function of Z versus N. The most promiment features in the figure are the sharp peaks that occur for N=Z=12, 14, 20, and 28. These pillars of stability are manifestations of the above-mentioned Wigner effect. The $N = 28$ shell gap can be seen to decrease between the values $Z = 20$ and 28 but still remains relatively strong (around 5 MeV). The feature of Fig. 2 of particular relevance for this paper is the steady decline of the $N = 20$ empire towards the dripline (i.e., with decreasing Z), practically to extinction.

The question of (vanishing) shell strength is obviously critical for the existence of superheavy elements. Recent

heroic experimental efforts have resulted in the discovery of isotopes of the elements $114-116$ [39,40], but it remains to be seen whether $Z = 114$ and $N = 184$ are indeed magic.

Whether the so-called magic numbers retain their supernatural power as we proceed to the drip line is also a question of great interest to astrophysics, specifically to the r process, thought to be responsible for the production of over half of our heavy elements. The observed solar system r-process abundances show pronounced peaks correlated to the classic magic neutron numbers 50, 82, and 126. It is a longstanding question as to whether the abundance troughs that preceed these peaks are due to astrophysical conditions or rather to nuclear physics, specifically the role of possible shell "quenching" [41–43].

The above questions, and others associated with the role of the binding energy, are discussed at length in a recent review article [44].

Mass measurements first brought the phenomenon of shell instability into the arena for study and naturally, continue to provide constraints and insight into questions on nuclear structure. Mass spectrometry, like the abovementioned experimental techniques, has also enjoyed a renaissance (see e.g. [44,45]). The MISTRAL [2] experiment has enabled us to return to the origin of this interesting physics problem by examining, with unprecedented accuracy, the neutron separation energies of some of the exotic nuclides on and around the island of inversion. In a previous paper [12], we presented mass measurements for $^{26-30}$Na offering, in addition, a detailed description of the spectrometer and method. In this paper we present mass measurements made by MISTRAL of the isotopes $^{29-33}$Mg at the ISOLDE radioactive beam facility [46], made possible by use of the ISOLDE laser ion source [47–49]. In addition to providing good ionization efficiency, the chemical selectivity of the laser enormously suppresses isobaric contamination. The spectrometer itself is only briefly described, as is the calibration procedure, the details of which are the subject of an accompanying publication [51]. The results are compared to previous measurements, including a preliminary ^{32}Mg MISTRAL value obtained using the plasma ion source [52,53], and discussed in light of the shell-opening problem.

2 Description of the MISTRAL spectrometer

The MISTRAL spectrometer has been described elsewhere [12,52–57]. The mass is determined via the cyclotron frequency f_c of an ion of charge q and mass m, in a homogeneous magnetic field B:

$$f_c = \frac{q\,B}{2\pi\,m} \tag{3}$$

The lay-out of MISTRAL is shown in Fig. 3. The ion beam follows a two-turn helicoidal trajectory (Fig. 3, inset center) to a secondary electron multiplier for counting. In order to obtain the high resolution needed for a precision mass measurement, a modulation of the longitudinal ion kinetic energy is effected by applying a time-varying (radiofrequency) voltage after one and three half-turns inside the magnetic field (Fig. 3, inset right). The ions thus make one cyclotron orbit between the two modulations. The ions are maximally transmitted through the 0.4 mm exit slit when the net effect of the two modulations is zero. This happens when the radiofrequency voltage is an integer-plus-one-half multiple of the cyclotron frequency:

$$f_{RF} = (n + \frac{1}{2})\, f_c \tag{4}$$

The ion signal recorded over a wide frequency scan will exhibit transmission peaks that are evenly spaced at the cyclotron frequency (Fig. 3, inset left). The resolving power $R = m/\Delta m$, will depend on the harmonic number n, the exit slit half-width w, and the modulation amplitude, D_m of the trajectory diameter [56]:

$$R = 2\pi n \frac{D_m}{w} \tag{5}$$

The value of n is typically a few thousand and w is $\pm$ 0.2 mm. Depending on the ion velocity and modulator frequency response, D_m can vary between 3 and 6 mm. D_m is then proportional to the product of the modulation efficiency and the applied voltage. (See [52] for more detailed discussion.)

Fig. 3, (inset left) shows a recorded transmission signal of the 60 keV ISOLDE ^{24}Mg beam over two successive harmonic values. As the RF power is increased, the voltage on the modulator increases (as the square root) and the conditions for transmission become more and more restrained, to the point where the wings of the transmitted ion signal can be completely suppressed. This happens when the modulation amplitude exceeds the width of the "phase definition slit," located between the entrance and exit slits, to eliminate modulated ion trajectories with large radial excursions. By closing the phase definition slit, it is possible to extend the zero-background zone which can be important in cases where isobaric contamination is present (as it was in the case of a previous measurement of ^{32}Mg [52,53].) Note however that this comes at a reduction of signal intensity: to have about half the area between harmonics background free requires paying about 60% in transmission and a factor of ten must be sacrificed to achieve a background-free zone of over 80%. The resulting peak shape is approximately triangular [53,56,57]. The resolving power obtained for the two cases shown in Fig. 3, (inset left) is 20,000 and 70,000 for the lower curve. A resolving power of 10^5 has been achieved.

The transmission of the spectrometer (through the four 0.4 mm $\times$ 5 mm slits that precisely define the nominal trajectory) is about 0.5% using the surface ionization reference source but can be lower than 0.01% using ISOLDE ion sources. In cases where higher resolving power is necessary (e.g. isobaric contamination), the cost in transmission can be a further order of magnitude.

MISTRAL relies on a comparative measurement of a (generally stable) reference nuclide of well-known mass.

[2] Mass measurements at ISOLDE using a Transmission and Radiofrequency spectrometer on-Line

The unknown mass m_x is transmitted through the spectrometer alternately with a reference mass m_r - without changing the magnetic field. Comparing masses in this way requires changing the transport energy of the reference beam, and with it, the voltages of all electrostatic elements in the spectrometer, according to the relation:

$$m_r V_r = m_x V_x \ . \tag{6}$$

These comparisons are done in rapid succession (seconds) in order to eliminate error contributions due to the long-term drift of the magnetic field.

3 Production of the exotic Mg nuclides

Exotic nuclides are produced at the ISOLDE facility by nuclear reactions induced by an incident pulse of 1.0 or 1.4 GeV protons. These pulses, containing up to 3×10^{13} protons, are positioned within a timing structure called the PS supercycle, usually containing 12 pulses, spaced every 1.2 seconds. On average, about half of these pulses are sent to ISOLDE.

Once created, radioactive atoms diffuse into a chamber where they are ionized. Three possibilities exist depending on the chemical nature of the element in question: surface ionization, plasma-discharge, or resonant laser ionization. The target-ion source unit is operated on a high voltage platform so that once ionized, the exotic nuclides are accelerated (normally to 60 keV) and mass separated. A general description of the ISOL technique is given in [46] and [44].

The data presented in this paper were recorded in September 2001 using the ISOLDE uranium carbide target combined with a resonant ionization laser ion source (RILIS) which delivers singly ionized, radioactive beams of exceptional chemical purity [47–49]. Some isobaric contamination from Na was present since it is surface ionized but the production cross-sections favor Mg by about a factor of 50 and the short Na half-lives suppress those yields by almost another order a magnitude. By blocking the laser beam, we performed a check measurement on ^{26}Na.

In a previous experiment [52,53], we used the plasma ion source in an attempt to measure the masses of several chemical species. Unfortunately, the isobaric contamination brought by the unselective plasma was overwhelming. In many cases, identification was even impossible due to the many possibilities of molecular sidebands as well as charge state. As a result, the resolving power of the spectrometer had to be increased to the point where a significant transmission loss made the measurements very difficult.

A comparison of recorded mass peaks for ^{32}Mg using the plasmas and laser ion sources, is shown in Fig. 4. The plasma peak (inset) was obtained by accumulating 20 pulses per frequency channel, correponding to 0.4 detected ^{32}Mg ions/pulse at maxiumum peak amplitude. The RILIS peak, containing 400 counts at the maximum, was accumulated from 50 pulses, corresponding to 8 ^{32}Mg ions/pulse at maximum amplitude. This twenty-fold increase is due to several factors. First, the beam purity afforded by RILIS allowed us to relax the resolving power, resulting in a gain of about four or five in transmission. (Note that while the plasma peak is less statistically abundant, its FWHM is half that of the laser peak and has zero background.) Assuming similar target performance (note that considerable variation can be possible), the RILIS performance would conceivably account for another factor of four to five improvement. The transmission of the laser-ionized ISOLDE beam through the spectrometer (without radiofrequency) was about three times better than the plasma-ionized beam, presumably due to a better ion source emittance. The remaining improvement may well be from a higher ionization efficiency of RILIS compared to plasma for Mg (see [49]).

4 Results

4.1 Calibration

In our Na paper [12], we showed how the relative differences $\Delta_x^{meas} = (m_x - m_x^{ame})/m_x^{ame}$ of measured masses m_x with those of the atomic mass evaluation m_x^{ame} [58] revealed a dependency on the difference between the MISTRAL reference mass m_r and the ISOLDE unknown mass m_x, presumably due to imperfect superposition of the m_x and m_r trajectories in the magnetic field that is known to have residual gradients [50].

The measurements are therefore corrected by a calibration, with an associated uncertainty. This calibration has been the source of intense study both on- and off-line and as such, is the subject of an independent publication [51]. The new calibration law, developed in [51], takes the form:

$$\Delta_x^{correct} = \Delta_x^{meas} - 2a(V_x - V_r)/(V_x + V_r) - b \tag{7}$$

The constant term b is added to correct for the offset which is observed between ISOLDE and MISTRAL beams of like mass.

In this experiment, a, b were determined by periodically measuring the precisely known masses ^{24,25,26,28}Mg as well as ^{23}Na with respect to an $A = 28$ reference beam of the singly ionized molecule ^{14}N^{14}N, throughout the run. A linear least-squares fit performed on the ensemble of calibration measurements resulted in the addition (in quadrature) of an error of 4×10^{-7}. The previous Mg measurements (using the plasmas source) [52,53], required an error of 12×10^{-7} (see discussion below). The details of the data analysis for this experiment, the calibration law in general, as well as the application of the new law to previously published data, are all discussed in the parallel publication [51].

4.2 Mass Values

The mass values are given in Table 1. The error includes the statistical and calibration errors (see detailed analysis in [51]).

Table 1. MISTRAL results. The first column corresponds to the nuclidic name. Column 2 gives the absolute deviations from the AME'95 mass table [58], and column 3, the new MISTRAL mass excess. Note that these values supersede those listed in the recent AME'03 mass table [60] which were based on a preliminary analysis using the old calibration law.

Nuclide	δm_x (keV)	Mass excess(keV)
Calibrant masses		
^{23}Na	2.6(5.5)	
^{24}Mg	−4.0(5.5)	
^{25}Mg	−3.9(7.0)	
^{26}Mg	5.7(6.1)	
^{28}Mg	−5.0(13.4)	
Measured masses		
^{29}Mg	52.8	−10609(14.8)
^{30}Mg	−9.9	−8892(9.5)
^{31}Mg	26.2	−3189(13.1)
^{32}Mg	−119.7	−916(20.1)
^{33}Mg	−256.8	4947(22.4)

The calibrant masses show excellent agreement with the 1995 "Atomic Mass Evaluation" (AME'95) [58] thereby confirming the validity of the method and calibration law. The relative precision for these masses is between 2 and 5×10^{-7} while for the measured masses it falls between 3 and 7×10^{-7}.

4.3 Evaluation

A significant improvement in the mass values has been achieved, especially far from stability, reaching almost an order of magnitude. Table 1 shows that the mass of ^{32}Mg is about 120 keV more bound, and that of ^{33}Mg is 257 keV more bound than the AME'95 values. To probe the reasons for this we examine in Fig. 5 the results of all experiments in which the masses of $^{30-33}$Mg were determined by direct techniques (the mass of ^{29}Mg was derived from two reactions) as well as the (overall) recommended mass values from the AME'95 [58], obtained from time-of-flight measurements at two installations: LAMPF [61, 62] and GANIL [63, 64].

Also compared in Fig. 5 is the 1999 MISTRAL measurement for ^{32}Mg using the plasma ion source [52,53]. Following that experiment, a discharge was discovered on the electrostatic injection septum and it is reasonable to assume that maintaining a congruence between the two trajectories would be impossible. Despite this problem, the 1999 results are in agreement with the new results, performed under quite different (and better) conditions.

Overall, the new MISTRAL measurements are quite compatible, not only with the previous individual measurements but also the recommended values from the 1995 evaluation (the slight deviation for the exotic ^{33}Mg is less than 2σ). However the uncertainty of the MISTRAL masses is five to seven times lower than those in the AME'95. As such, in the new AME'03 evaluation [60], the MISTRAL masses now account for 100% of the weight of the recommended values due to their superior precision. (Note that the values reported here supersede those listed in AME'03 [60] which were based on a preliminary analysis using a different calibration law.) In addition to the TOFI and SPEG values, some older reaction Q values (using ^{18}O and ^{11}B projectiles on ^{26}Mg targets) and Q_β values from exotic Na nuclides, no longer contribute due to their large uncertainties [60].

Any mass measurement has need of a calibration. In many cases, exotic masses are derived using extrapolations from nuclides closer to stability. Recent measurements of neutron-rich Mg isotopes (among others) at GANIL were reported in [4]. In that work, the (AME'95) mass of ^{33}Mg was used as a *calibrant* for the measured masses of $^{34-36}$Mg. If the calibration is off by 250 keV, this could have considerable impact on the mass values further from stability. In fact, the evaluators of the AME'03, considered that the masses of $^{34-36}$Mg deviated too much from smooth trends and consequently replaced them by systematic values.

5 Discussion

5.1 Comparison to Mass Models

Mass models can cover a wide spectrum, in terms of applicability as well as in terms of physics input. They can broadly be described as being either local in character, typically containing many parameters (adjusted to experimental masses) and predicting unknown masses with relatively good accuracy very close to the region where the ajustment was made. Global models tend to have fewer ajustable parameters and more physics. While this can make the predictions somewhat worse, the extrapolation to further unknown regions tends to be more reliable. See [44] for a general classification, explanation and comparison of the various types of models.

Predictions for Mg masses from the macroscopic-microscopic Finite Range Droplet Model (FRDM) of Moeller et al. [65], microscopic shell model calculations [66], as well as the microscopic mass formula of Duflo and Zuker (DZ95) [67], Koura et al. (KUTY) [68], and HFB-2 [69] are shown in Fig. 6, compared to the experimental values determined in this work. Perhaps the most striking feature of Fig. 6 is the odd-even staggering compared with experiment indicating a major problem in how the pairing force is handled by mass formulas in general (see discussion in [44]). The shell model calculations seem not to be affected by this, however after $N = 18$ they veer off towards the hopelessly underbound. This is very illustrative of restricted mathematical basis and coupling with continuum, two major problems besetting the shell model. The pairing problem seems quite pronounced for the FRDM and KUTY formulas while it is much less acute for DZ. Interestingly, the KUTY, FRDM and DZ formulae all show the same behavior crossing the $N = 20$ shell. Whether this shell is closed or not, the microscopic HFB–2 formula shows a strong underbinding. But on the whole, its 705 keV rms deviation for the Mg isotopes is comparable to that of KUTY (627

keV) and even better than FRDM (848 keV). [3] At 521 keV, the DZ formula does the best job in this region – as it does for the entire mass table (see [44]). The rms error for the shell model calculations is 1.2 MeV.

5.2 General Discussion

The impact of precision mass measurements on the question of shell opening is not particularly clear-cut. Like many results, they bring pieces of a large puzzle and in other cases, masses provide overall constraints that need to be satisfied by level assignments, half-life calculations, or model predictions.

The shell gap was discussed in the introduction and the mass surface discussed in this context. In the light region of $N = 20$, it is particularly difficult to disentangle the various structure effects from the mass surface since things change so quickly for small numbers of nucleons. In Fig. 7 the $N = 20$ shell gap is compared to predictions of some of the above models. This is an interesting exercise since the shell gap is calculated from mass *differences*. It might be possible for a model to follow the microscopic behavior fairly well despite having a large, but relatively constant difference.

Conspicuous in Fig. 7 is the large shell gap for $N = Z = 20$, a Wigner nuclide which is also doubly magic. All three models underestimate this effect (by at least 1 MeV). Contrary to the absolute mass values, the FRDM seems to follow the shell gap (i.e., mass difference) data relatively well. The shell opening is very sudden below $Z = 11$, moreover becoming negative! DZ95, despite its success with heavier shell gaps, predict a more gradual erosion of the shell gap. The HFB–2 results give us a shell opening already at $N = 13$ and seem to be systematically lower than experiment.

As mentioned in the introduction, the island of inversion has been intensely studied from both experimental and theoretical perspectives. The subject is very nicely introduced by the Pritychenko suite [30–34]. The first movement of this extended oeuvre [30], provided the first $B(E2)$ values for ^{26,28}Ne and ^{30,32}Mg, on the basis of which island residency permits were denied for all but ^{32}Mg. The permit of another long-standing resident, ^{31}Na was confirmed in the subsequent movement [31] in which the quadrupole moment was also determined. The next examination was for ^{34}Al, with the verdict concurring with the binding energy arguments: non-resident [32]. In [33], ^{33}Mg was vetted and found to possess a low-lying rotational state, having a deformation similar to the other island residents. However, this conclusion is different from that of the β-spectroscopy study of Nummela et al., [23]. Finally, in [34], the excitation cross-sections of ^{28,30}Na were measured and quadrupole moments found not to correspond to intruder ground state configurations, banishing these nuclides from the island. Previous (and more precise) measurements of the quadrupole moments of $^{26-31}$Na by a $\beta-$NMR, optical pumping technique at ISOLDE [28], are more or less in agreement. Curiously, the conclusion concerning the residency of ^{30}Na is the opposite.

The criterion for deciding whether a given nuclide is part of the island of inversion or not, is somewhat subjective. The older arguments derived from binding energies (e.g., [14]) could be questioned on one hand, by more precise mass data that has since become available [12,60], and on the other hand by more recent shell model calculations [66] that indicate a departure from the "universal sd shell" already at N=19 for Na (see discussion in [12]). This conclusion is supported by the quadrupole moment measurements from $\beta-$NMR [28]. The very recent results using $\beta-$NMR at ISOLDE for the magnetic moment and unambiguous ground-state spin of ^{31}Mg, coupled with state-of-the-art shell model calculations, also indicate the invasion of the intruder orbits at $N = 19$ [29].

The shell model calculations that accompanied the β-spectroscopy of ^{33}Mg in [23] included only an approximation of the mixing between $0p0h$ and $2p2h$ configurations. This apparently leads to an excited state of different instrinsic stucture than that described by the complementary Coulomb excitation studies in [33], namely that the excited state in question is rotational in nature, leading to different conclusions regarding the ground state spin and deformation. A more recent $\beta-$decay study of ^{33}Mg by [24] has also made different assumptions regarding the configuration of the ground state.

Further discussion of these differing conclusions is beyond the scope of this paper. (Note that the discussion of this question by Morten et al., [24] ends with the statement: "More details of the experimental decay scheme and more complete shell model calculations are required for an understanding of the ^{33}Mg structure.") However, the importance of different, complementary experimental techniques is clear enough. [4] The eagerly awaited results from REX-ISOLDE [38] are sure to shed new light on the current troublesome situation.

6 Conclusion

We have discussed the results for the masses of neutron-rich Mg isotopes using a new technology for mass measurements that is especially suitable for very short-lived species. The results represent the most accurate measurements to date for the short-lived nuclides $^{29-33}$Mg which lie in the so-called "island of inversion" around the $N = 20$ shell closure. The measurements not only confirm the previous values but even show an enhancement of the binding energy which further emphasizes the quenching of the

[3] Note, however, that the parameters of HFB–2 were adjusted to a more extensive data set than the others (see [69, 44]).

[4] Interestingly, Nummela et al., [23] report that the uncertainties related to building the level schemes for ^{33}Mg are dominated by the error on the ^{33}Na-^{33}Mg $Q-$value. In the same vein, Mantica et al., [7,8] remind us that the errors in half-life calculations are dominated by Q-value uncertainties. Hence, the importance of precision mass measurements is not understated.

normally-stabilizing "magic" number shell effect. It is perhaps indicative of the persistence of this problem that we retain the unscientific term "magic". We have examined this curious phenomenon in light of recent mass models, find that if evanescent shell stability is to be properly included for studying the astrophysical r process, then improvements will have to be made. This is tantamount to the requirement for more mass data, farther from stability.

Efforts are currently underway to increase the sensitivity of the spectrometer. These improvements will allow MISTRAL to realize its full potential for accurate mass measurements of the shortest-lived nuclides approaching the drip line and the manifestation of this curious phenomenon of magic number migration.

7 Acknowledgements

We would like to acknowledge the expert technical assistance of G. Conreur, M. Jacotin, J.-F. Képinski and G. Le Scornet from the CSNSM. We also express our sincere gratitude to V.N. Fedoseyev and D.V. Fedorov for the superbly reliable operation of the laser ion source, and to T. Giles, U. Köster, H. Fynbo and L. Weissman for their symbiotic help in tuning the ISOLDE HRS separator. We thank H. Doubre for his assistance during the experiment. The MISTRAL program is supported by France's IN2P3 and by the EU research network NIPNET (contract number HPRI-CT-2001-50034). The work at ISOLDE was partially supported by the EU RTD program "Access to Research Infrastructures," under contract number HPRI-CT-1998-00018.

References

1. C. Thibault, R. Klapisch, C. Rigaud, A. M. Poskanzer, R. Prieels, L. Lessard and W. Reisdorf, Phys. Rev. C 12 (1975) 644
2. A. Ozawa, T. Kobayashi, T. Suzuki, K. Yoshida, I. Tanihata, Phys. Rev. Lett. 84 (2000) 5493
3. S. Shimoura et al., Phys. Lett. B 560 (2003) 31
4. F. Sarazin et al., Phys. Rev. Lett. **84** (2000) 5062
5. R. Kanungo, I. Tanihata, A. Ozawa, Phys. Lett. B 528 (2002) 58
6. J.I. Prisciandoaro et al., Phys. Lett. B 510 (2001) 17
7. P.F. Mantica et al., Phys. Rev. C 67 (2003) 014311
8. P.F. Mantica et al., Phys. Rev. C 68 (2003) 014311
9. D.E. Appelbe et al., Phys. Rev. C 67 (2003) 034309
10. R.V.F. Janssens et al., Phys. Lett. B 546 (2002) 55
11. O. Sorlin et al., Phys. Rev. Lett. 88 (2002) 092501
12. D. Lunney, G. Audi, H. Doubre, S. Henry, C. Monsanglant, M. de Saint Simon, C. Thibault, C. Toader, C. Borcea, G. Bollen and the ISOLDE Collaboration, Phys. Rev. C 64 (2001) 054311
13. K. Heyde, J.L. Wood, J. Phys. G: Nucl. Part. Phys. 17 (1991) 135
14. E.K. Warburton, J.A. Becker, B.A. Brown, Phys. Rev. **C 41** (1990) 1147.
15. Y. Utsuno et al., Phys. Rev. C 60 (1999) 054315
16. T. Otsuka et al., Phys. Rev. Lett. 87 (2001) 082502
17. T. Suzuki, R. Fujimoto, T. Otsuka, Phys. Rev. C 67 (2003) 044302
18. P.D. Stephenson, J. Rikovska-Stone, M.R. Strayer, Phys. Lett. B 545 (2002) 291
19. M. Yamagami and N. Van Giai, Phys. Rev. C 69 (2004) 034301
20. G. Gori et al., Phys. Rev. C 69 (2004) 041302(R)
21. C. Détraz, M. Langevin, M. C. Goffri-Kouassi, D. Guillemaud, M. Epherre, G. Audi, C. Thibault and F. Touchard, Nucl. Phys. **A 394** (1983) 378
22. D. Guillemaud-Mueller, C. Détraz, M. Langevin, F. Naulin, M. de Saint Simon, C. Thibault, F. Touchard and M. Epherre, Nucl. Phys. **A 426** (1984) 37
23. S. Nummela et al., Phys. Rev. C 64 (2001) 054313
24. A.C. Morton, P.F. Mantica, B.A. Brown, A.D. Davies, D.E. Groh, P.T. Hosmer, S.N. Liddick, J.I. Prisciandaro, H. Schatz, M. Steiner, and A. Stolz Phys. Lett. B 544 (2002) 274
25. J. Enders et al., Phys. Rev. C 65 (2002) 034318
26. W. Mittig et al., Eur. Phys. J. A 15 (2002) 157
27. T. Motobayashi, Eur. Phys. J. A 15 (2002) 99
28. M. Keim, in *Proceedings of the International Conference on Exotic Nuclei, Atomic Masses (ENAM98),* AIP Conf. Proc. No. 455, edited by B.M. Sherrill, D.J. Morrissey, and C.N. Davids, (AIP, New York, 1998), p. 50.
29. G. Neyens, M. Kowalska, D. Yordanov et al., Phys. Rev. Lett. (2004) submitted
30. B.V. Pritychenko et al. Phys. Lett. **B 461** (1999) 322.
31. B.V. Pritychenko, T. Glasmacher, B.A. Brown, P.D. Cottle, R.W. Ibbotson, K.W. Kemper, L.A. Riley, H. Scheit, Phys. Rev. C 63 (2000) 011305(R)
32. B.V. Pritychenko et al., Phys. Rev. C 63 (2001) 047308
33. B.V. Pritychenko et al., Phys. Rev. C 65 (2002) 061304(R)
34. B.V. Pritychenko et al., Phys. Rev. C 66 (2002) 024325
35. V. Chisté et al., Phys. Lett. B 514 (2001) 233
36. K. Yoneda et al., Phys. Lett. B 499 (2001) 233
37. H. Iwasaki et al., Phys. Lett. B 522 (2001) 227
38. H. Scheit and the REX-ISOLDE and MINIBALL Collaborations, Proceedings of RNB6, Nucl. Phys. A (2004) in print; Experimental proposal CERN-INTC-2004-009 (2004)
39. Yu. Ts. Oganessian et al., Phys. Rev. C 69 (2004) 054607
40. Yu. Ts. Oganessian et al., Phys. Rev. C 69 (2004) 021601(R)
41. B. Chen et al., Phys. Lett. B **355** (1995) 37
42. J.M. Pearson, R.C. Nayak, and S. Goriely, Phys. Lett. **B387** (1996) 455
43. K.-L. Kratz, B. Pfeiffer, F.-K. Thielemann, W. B. Walters, Hyperfine Interact. 129 (2000) 185
44. D. Lunney, J.M. Pearson, C. Thibault, Rev. Mod. Phys. 75 (2003) 1021
45. Proceedings of the 2nd Euroconference on Atomic Physics at Accelerators : Mass Spectrometry (APAC2000), Cargèse (France), D. Lunney, G. Audi, H.-J. Kluge, editors, Hyp. Int. 132 (2001)
46. E. Kugler, Hyperfine Interact. 129 (2000) 23
47. V.I. Mishin et al., Nucl. Instr. Meth. B 73 (1993) 550
48. V.N. Fedoseyev et al., Hyp. Interactions 127 (2000) 409
49. U. Koester, Nucl. Phys. A 701 (2002) 441
50. A. Coc et al., Nucl. Instr. Meth. A 305 (1991) 143
51. C. Gaulard, N. Vieira, G. Audi, C. Bachelet, D. Lunney, M. de Saint Simon, C. Thibault, submitted for publication (2004)
52. D. Lunney et al., Hyperfine Interact. 132 (2001) 299

53. C. Monsanglant, Doctoral Thesis #6283, Université Paris-Sud, Orsay, 2000; http://csnwww.in2p3.fr/AMDC/experimental/th-monsangl.pdf
54. M. de Saint Simon et al., Phys. Scripta **T59** (1995) 406.
55. M.D. Lunney et al., Hyp. Int. **99** (1996) 105.
56. A. Coc, R. Le Gac, M. de Saint Simon, C. Thibault, F. Touchard, Nucl. Instr., Meth. **A 271** (1988) 512.
57. N. Vieira, Doctoral Thesis, Université Paris VI, Paris, 2002
58. G. Audi, A.H. Wapstra, Nucl. Phys. **A 595** (1995) 409
59. G. Audi, A.H. Wapstra, private communication (2001). This unpublished table is a mid-stream evaluation that includes some mass values derived from systematic trends.
60. G. Audi, A.H. Waptstra and C. Thibault, Nuc. Phys. A729 (2003) 337; A.H. Waptstra, G. Audi and C. Thibault, Nuc. Phys. A729 (2003) 129
61. D.J. Vieira et al., Phys. Rev. Lett. **57** (1986) 3253.
62. X.G. Zhou et al., Phys. Lett. **B 260** (1991) 285.
63. A. Gillibert et al., Phys. Lett. **B 192** (1987) 39.
64. N.A. Orr et al., Phys. Lett. **B 258** (1991) 29, erratum Phys. Lett. **B 271** (1991) 468.
65. P. Möller, J.R. Nix, W.D. Myers, and W.J. Swiatecki, At. Data Nucl. Data Tables **59** (1995) 185.
66. E. Caurier, F. Nowacki, A. Poves, J. Retamosa, Phys. Rev. **C 58** (1998) 2033.
67. J. Duflo and A.P. Zuker, Phys. Rev. C 52 (1995) R1
68. H. Koura and M. Uno and T. Tachibana and M. Yamada, Nucl. Phys. A 674 (2000) 47
69. S. Goriely, M. Samyn, J.M. Pearson, P.-H. Heenen and F. Tondeur, Phy. Rev. C 66 (2002) 024326

Fig. 1. Two-neutron separation energy S_{2n} for elements up to $Z \sim 50$, as a function of neutron number N. Data are taken from [60]. Note the x-axis is plotted on a log scale to facilitate comparison of the shell closures at N =20, 28, and 50.

Fig. 2. Neutron shell gap Δ_N over the $N - Z$ plane for light nuclides calculated from experimental mass values taken from [59].

Fig. 3. Layout of the MISTRAL spectrometer (overhead view). The ion beams (coming from the right) are injected either from the ISOLDE beamline (at 60 keV) or from a reference ion source (variable energy). Inset (center) shows an isometric view of the trajectory envelope with the 0.4 mm injection slit followed by the first modulator after one-half turn, an opening to accommodate the modulated-ion trajectories after one-turn, the second modulator after three-half turns, and the exit slit. Inset (right) schematically illustrates the modulator electrode structure. Inset (left) shows the recorded signal of transmsitted ^{24}Mg 60 keV ISOLDE ions as a function of modulation frequency for two RF power settings. The higher curve shows a resolving power of 20,000 while the one with half the signal amplitude illustrates a resolving power of over 70,000.

Fig. 4. Reconstructed peaks for ^{32}Mg using the laser ion source (RILIS) and (inset) using the plasma ion source [52,53]. These measurements are sums of series of (random) frequency steps with each step recorded after the impact of a proton pulse on the ISOLDE target. The mass resolving power for the RILIS case is about 30,000 whereas 68,000 was used for the plasma source due to presence of isobaric contamination (note the zero background as well). The statistics (in the maximum channel) correspond to 50 proton pulses (8 ^{32}Mg ions per pulse) for RILIS and 20 pulses (0.4 per pulse) for the plasma.

Fig. 5. Comparison of the results of experiments in which the masses of $^{30-33}$Mg have been determined: time-of-flight measurements (TOF) at LAMPF [61],[62] and GANIL [63], [64] and RF mass spectrometry (this work).

Fig. 6. Comparison of the the newly measured Mg masses compared to predictions of several mass models (Shell98 [66], KUTY [68], FRDM [65], DZ95 [67], HFB–2 [69]).

Fig. 7. Comparison of the shell gap calculated by nuclear models (FRDM [65], DZ95 [67], HFB–2 [69]) and experiment [60].

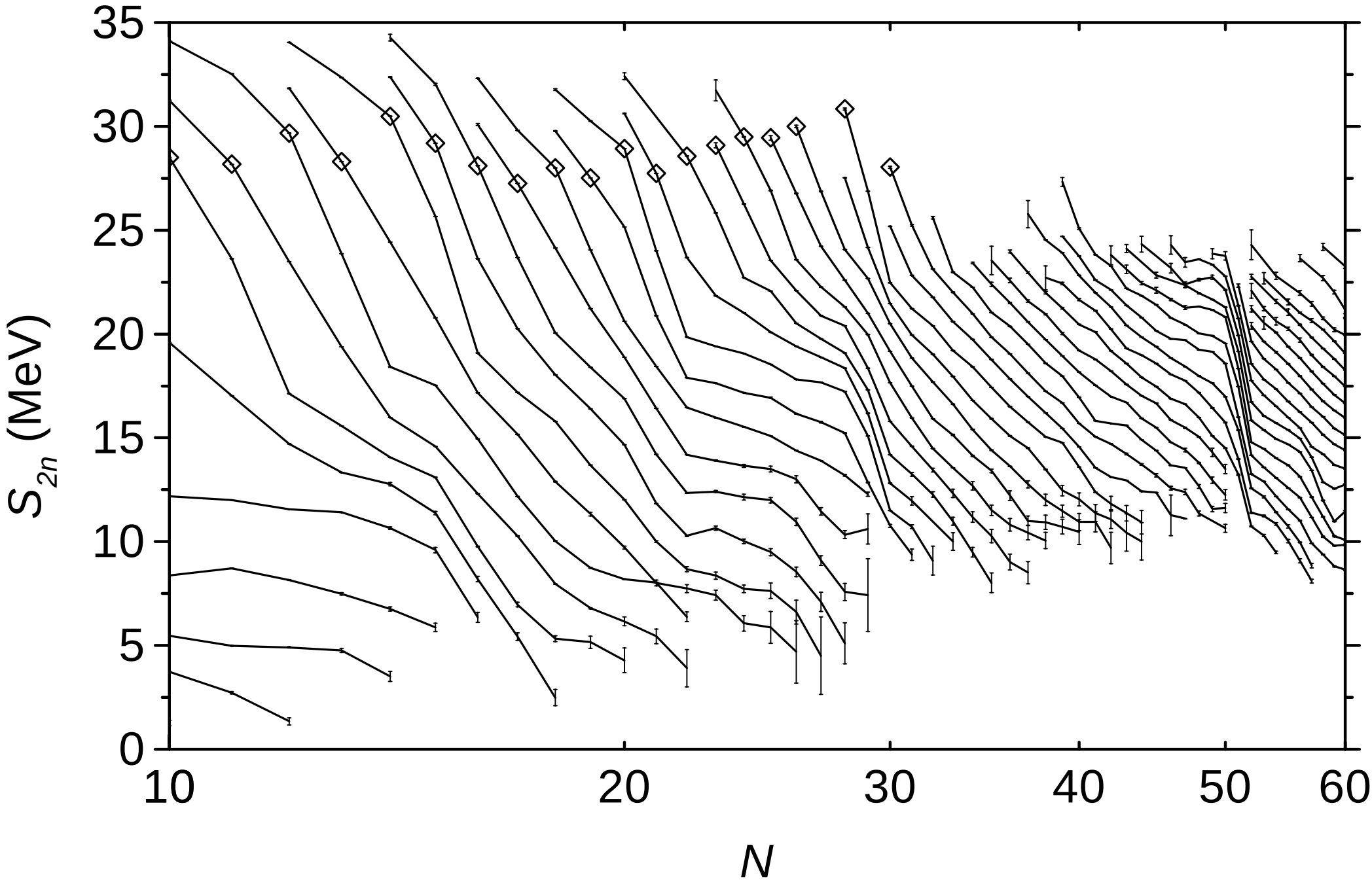
35
30
25
20
15
10
5
0
S_{2n} (MeV)
10
20
30
40
50
60
N

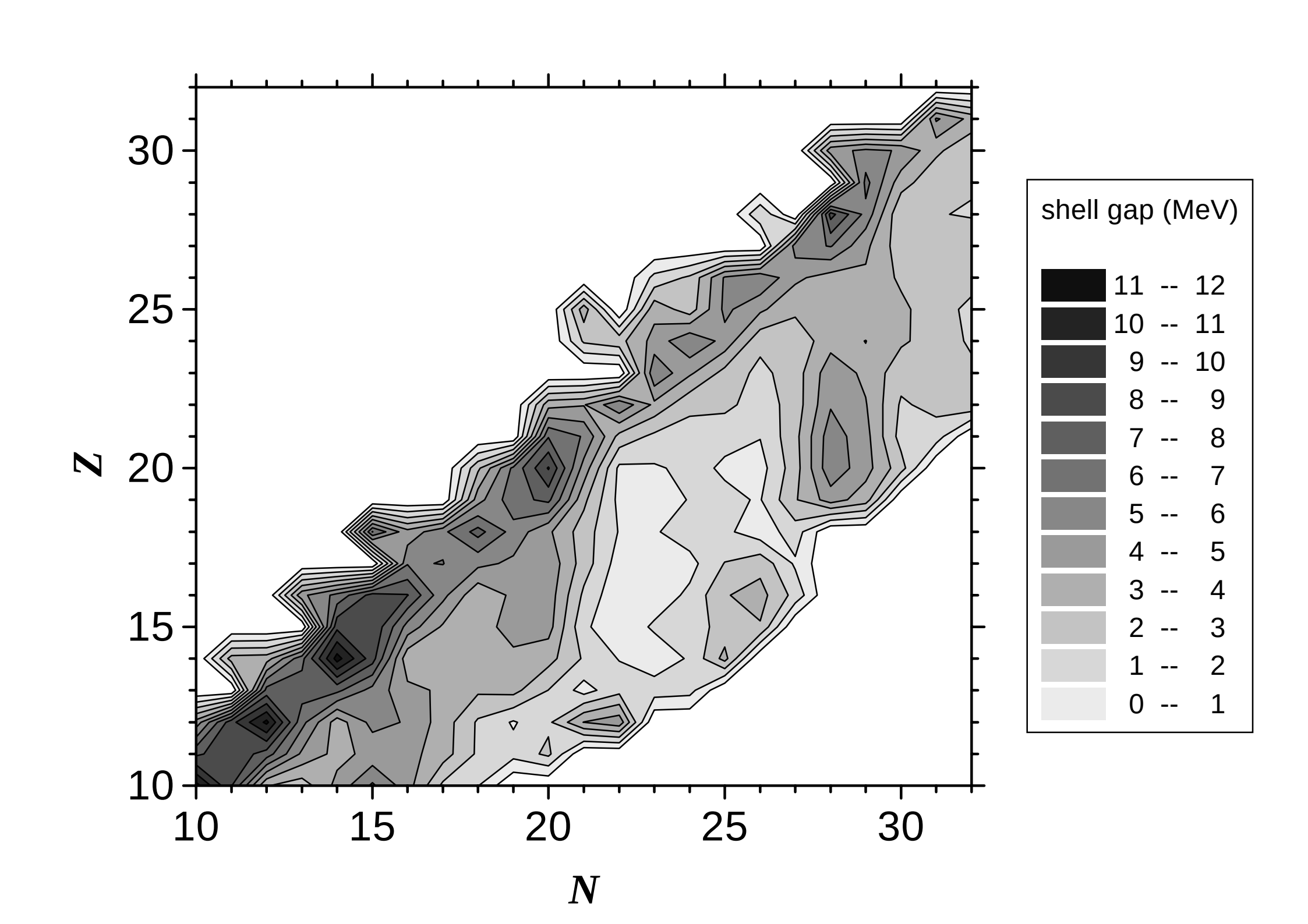
shell gap (MeV)
11 -- 12
10 -- 11
9 -- 10
8 -- 9
7 -- 8
6 -- 7
5 -- 6
4 -- 5
3 -- 4
2 -- 3
1 -- 2
0 -- 1
Z
N
10
15
20
25
30

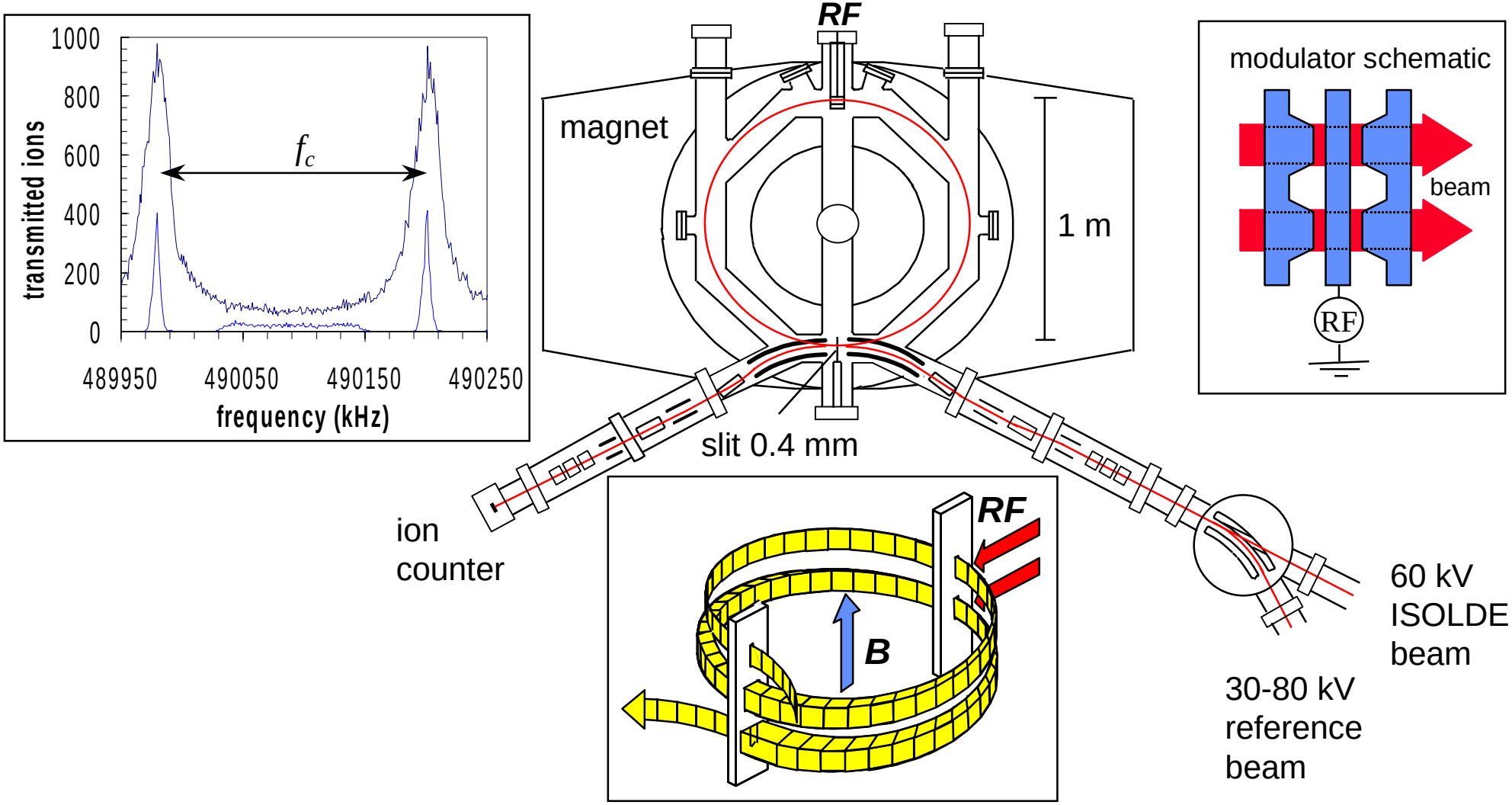
1000
800
600
400
200
0
transmitted ions
f_c
489950
490050
490150
490250
frequency (kHz)
RF
magnet
1 m
modulator schematic
beam
RF
slit 0.4 mm
ion
counter
RF
B
60 kV
ISOLDE
beam
30-80 kV
reference
beam

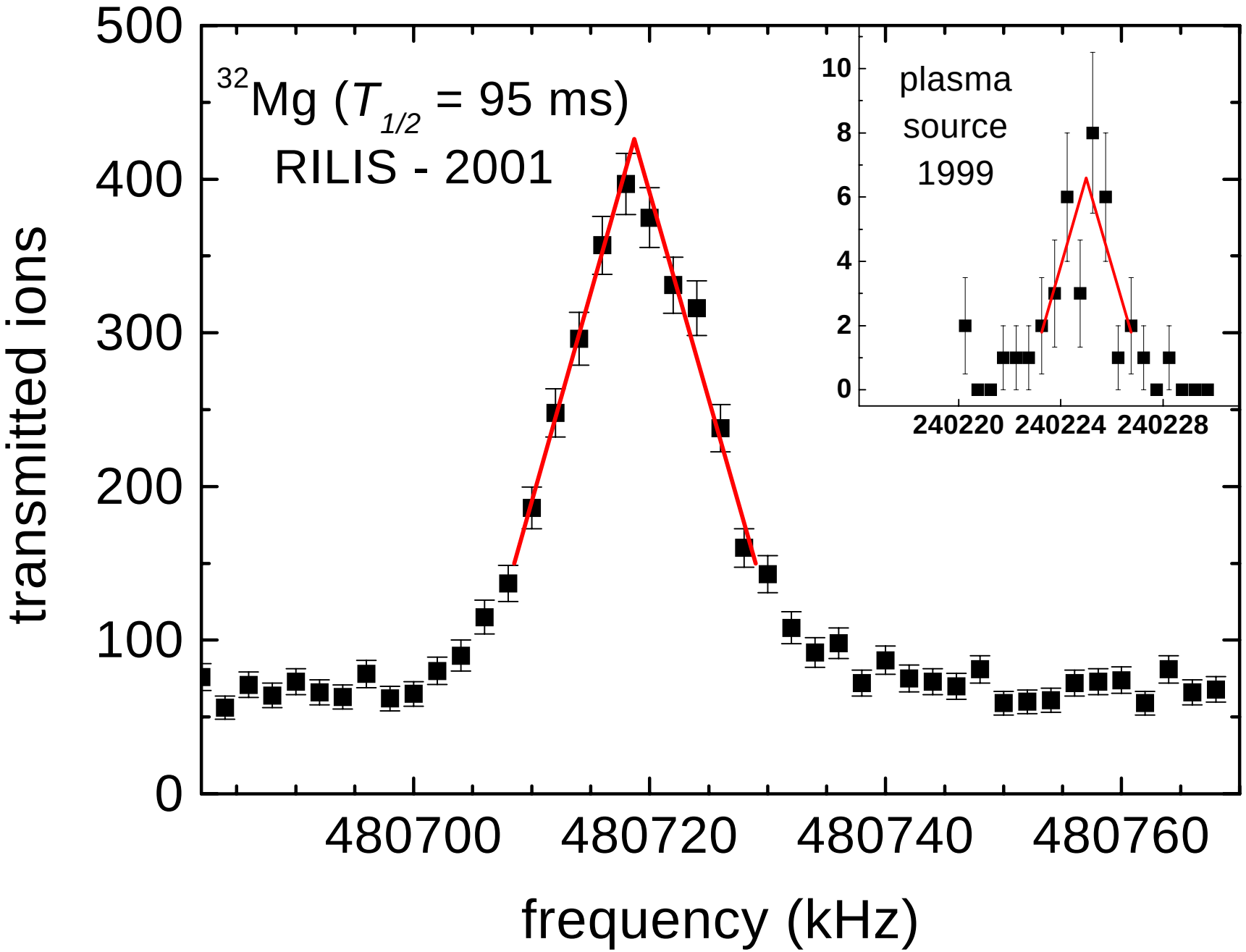
^{32}Mg ($T_{1/2}$ = 95 ms)
RILIS - 2001
plasma
source
1999
transmitted ions
frequency (kHz)
0
100
200
300
400
500
480700
480720
480740
480760
0
2
4
6
8
10
240220
240224
240228

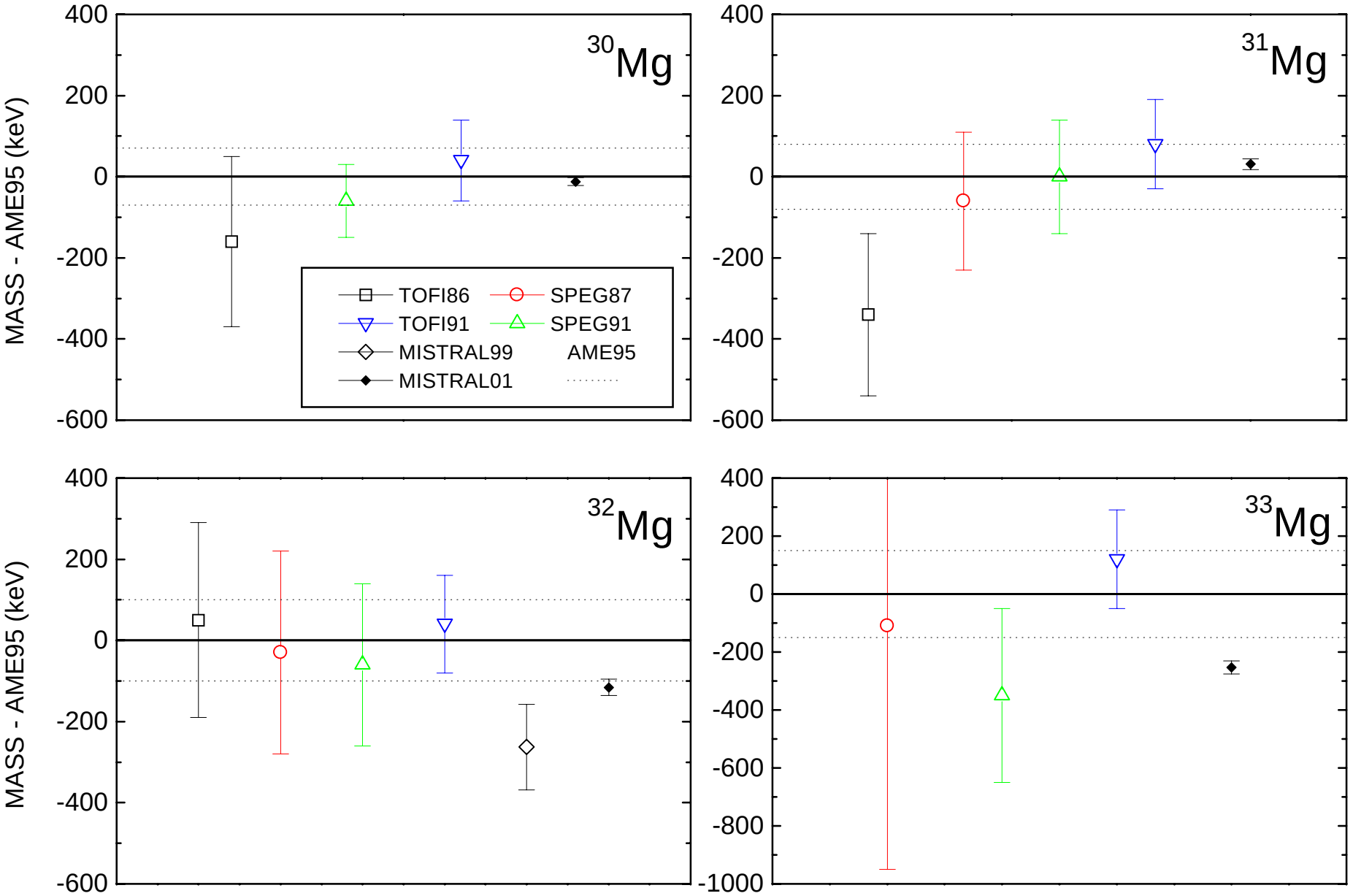
MASS - AME95 (keV)
400
200
0
-200
-400
-600
^{30}Mg
TOFI86
SPEG87
TOFI91
SPEG91
MISTRAL99
AME95
MISTRAL01
^{31}Mg
^{32}Mg
^{33}Mg
-800
-1000

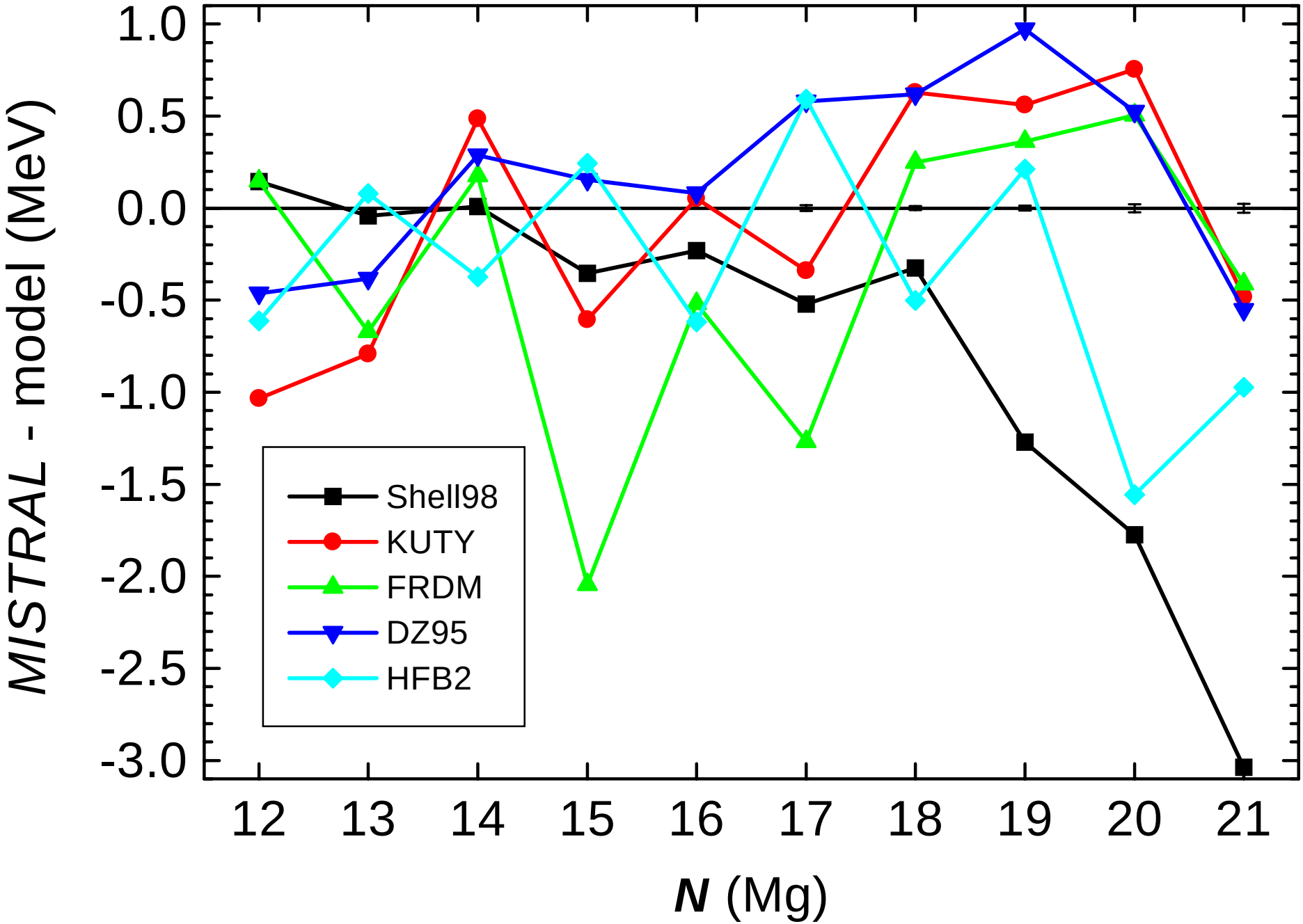
1.0
0.5
0.0
-0.5
-1.0
-1.5
-2.0
-2.5
-3.0
MISTRAL - model (MeV)
12
13
14
15
16
17
18
19
20
21
N (Mg)
Shell98
KUTY
FRDM
DZ95
HFB2

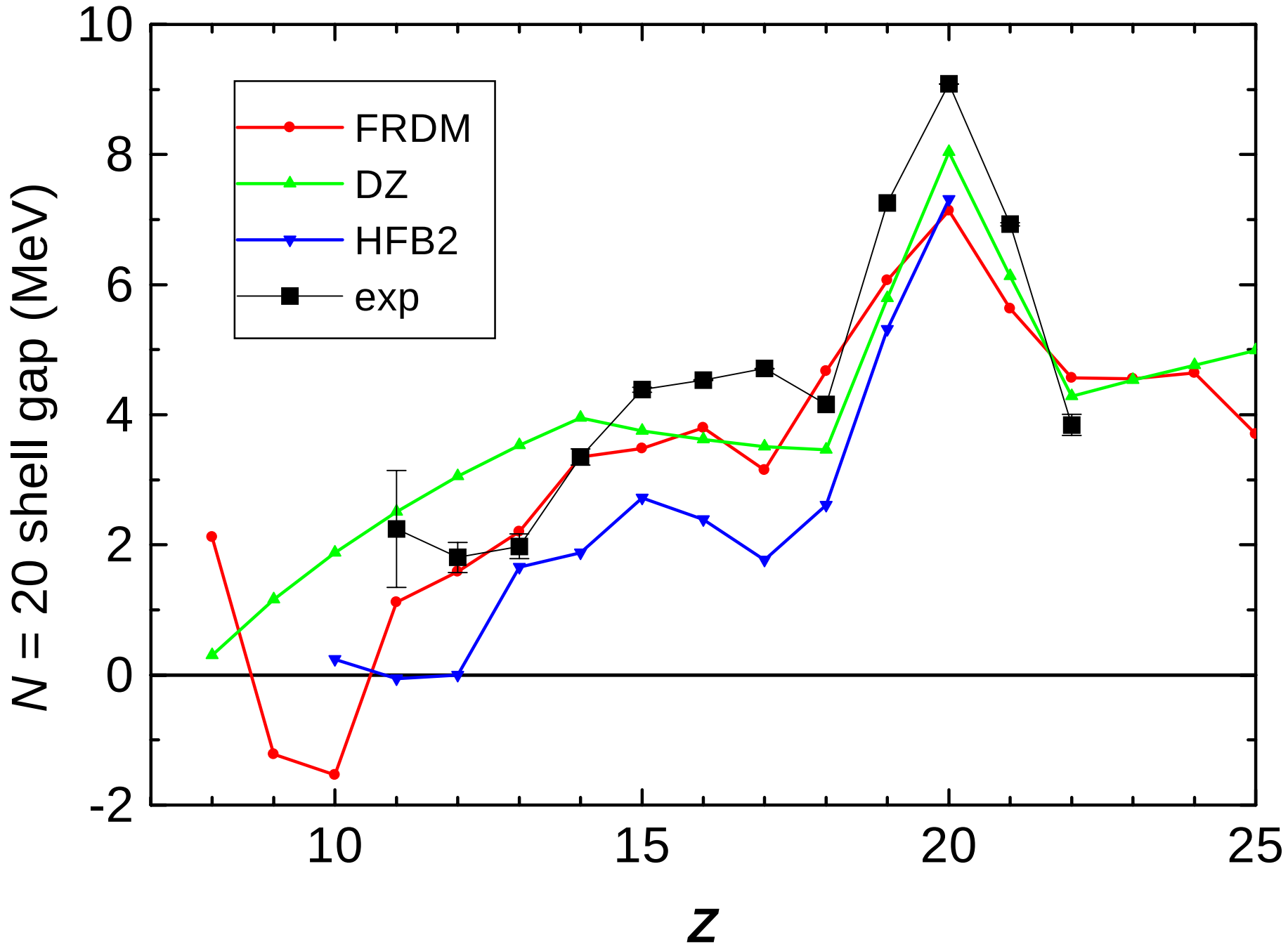
FRDM
DZ
HFB2
exp
10
8
6
4
2
0
-2
10
15
20
25
N = 20 shell gap (MeV)
Z